catalysts

MDPI

Article

Zirconium Phosphate Heterostructures as Catalyst Support in Hydrodeoxygenation Reactions

Daniel Ballesteros-Plata, Antonia Infantes-Molina *, Elena Rodríguez-Aguado, Pilar Braos-García, José Jiménez-Jiménez and Enrique Rodríguez-Castellón *

Departamento de Química Inorgánica, Cristalografía y Mineralogía (Unidad Asociada al ICP-CSIC), Facultad de Ciencias, Universidad de Málaga, Campus de Teatinos, 29071 Málaga, Spain; daniel.ballesteros@uma.es (D.B.-P.); aguadoelena5@gmail.com (E.R.-A.); mdbraos@uma.es (P.B.-G.); jjimenez@uma.es (J.J.-J.)

* Correspondence: ainfantes@uma.es (A.I.-M.); castellon@uma.es (E.R.-C.); Tel.: +34-952-131-877 (A.I.-M.); +34-952-131-873 (E.R.-C.)

Academic Editor: Monica Pica
Received: 30 April 2017; Accepted: 27 May 2017; Published: 2 June 2017

Abstract: A porous phosphate heterostructure (PPHs) formed by a layered zirconium(IV) phosphate expanded with silica galleries was prepared presenting a P/Zr molar ratio equal to 2 and a (Si + Zr)/P ratio equal to 3. This pillared zirconium phosphate heterostructure was used as a catalyst support for bi-functional catalysts based on noble metals (Pt or Pd) and molybdenum oxide containing a total metallic loading of 2 wt % and Pt(Pd)/Mo molar ratio equal to 1. The catalysts prepared were characterized by different experimental techniques and evaluated in the hydrodeoxygenation (HDO) reaction of dibenzofuran (DBF) as a model compound present in biomass derived bio-oil, at different reaction pressures. The catalyst characterization evidenced that a high dispersion of the active phase can be achieved by using these materials, as observed from transmission electron microscopy (TEM) characterization, where the presence of small particles in the nanometric scale is noticeable. Moreover, the textural and acidic properties of the phosphate heterostructure are barely affected by the incorporation of metals into its structure. Characterization results evidenced that the presented material is a good candidate to be used as a material support. In both cases, high conversions and high selectivities to deoxygenated compounds were achieved and the active phase played an important role. Thus, Pt/Mo presented a better hydrogenolysis capability, being more selective to O-free products; whereas, Pd/Mo showed a greater hydrogenation ability being more affected by changes in pressure conditions.

Keywords: hydrodeoxygenation (HDO); dibenzofuran; noble metals; molybdenum; pillared zirconium phosphate heterostructures

1. Introduction

Biomass is considered as a better and inexpensive alternative for decreasing the environmental impact produced by the burning of fossil fuels [1]. The pyrolysis of lignocellulosic biomass [2,3] made of cellulose, hemicellulose, and lignin leads to a dark brown highly viscous and dense liquid named bio-oil. This bio-oil contains molecules with a very different chemical nature [4] and presents a high oxygen content (>40%) [5]. These O-containing molecules confer deleterious properties such as high viscosity, poor heating value, immiscibility with hydrocarbon fuels, thermal instability, high corrosiveness and undesirable coke formation [6,7].

To increase bio-oil quality, some method refinements have been developed in recent years, of which the most attractive in terms of quality and price [8] is hydrodeoxygenation (HDO) under high pressure and moderate temperature (250–600 °C) conditions, in the presence of bi-functional catalysts [2], i.e., metal and acidic functions. In this form, oxygen present in the bio-oil is removed,

improving the quality of the bio-oil to be used in the internal combustion process [9]. Another important advantage of the HDO process is that refineries have adequate infrastructure to carry out these reactions [10].

Initially, HDO reactions were carried out with traditional catalysts used in refineries, as were transition metal catalysts (Ni, Co, Mo) supported on gamma alumina, which were pre-sulfides to increase their catalytic activity [11,12]. The problem of these catalysts is the release of sulfur compounds during the HDO reaction losing activity and also poisoning due to coke deposition on their surface [8,9].

Noble metals have presented very interesting results in hydrotreating, and therefore in HDO reactions [13,14]. To increase the activity of these catalysts, other researchers have based their studies in mono and bimetallic noble metal catalysts such as Rh, Ru, Pt or Pd, which reported good activation of hydrogen, no sulfur requirement in the feed and showed high conversions with long life-times [9,15–18]. The main handicaps are their high cost and the high hydrogen consumption. However, it is possible to decrease costs by synthesizing bimetallic catalysts of non-noble metals, such as cheaper transition metals, with a small charge of noble metal, obtaining good catalytic results in HDO reactions [2,13,19]. In previous papers, it was reported that both Pd and Pt presented limited activity for deoxygenation to yield hydrocarbons compared to Ru [20,21], both of them considered as good hydrogenating catalysts. Moreover, Wang et al. [20] observed that Pt showed superior hydrogenation (HYD) activity in the HDO reaction of DBF compared with Pd.

On the other hand, molybdenum presented interesting results as active phase in the HDO reaction of m-cresol. Its activity is directly related to the support employed, being highly selective to the direct deoxygenation route (DDO) [22]. These authors concluded that the most reactive materials were those supported on ZrO_2 and TiO_2 that favor the formation of Mo(V) or Mo(III) species. Moreover, some authors obtained high HDO activity and selectivity towards non-oxygenated biomass products [23,24]. Román-Leshkov et al. [22] found that MoO_3 is active and selective in HDO with hydrogen pressures of 1 bar and temperatures at 300 °C. The MoO_3 catalyst showed a high tolerance to coke formation and was also regenerated by calcination without loss of activity. They further found that the catalyst was gradually deactivated due to the formation of inactive Mo(IV) upon reduction. In a later study, the presence of Mo(V) species on the surface of the catalyst was found to act as a Lewis acid site that weakened the C-O bond upon adsorption of the molecule on the active site [25]. The influence of Mo in HDO reactions indicates that it increases the selectivity toward deoxygenated products shown by PtMo catalyst with respect to the monometallic one, where the Mo seems to introduce a new preferred pathway by changing the kinetic barriers [26]. So these studies suggest that molybdenum-based catalysts have unique properties that make them suitable for use as HDO catalysts.

Considering the material support, a great variety of supports have been evaluated such as TiO_2, ZrO_2, SiO_2 or ZSM-5 [8,15,16,22,27,28]. More recently, the layered double hydroxides (LDH) and their derived metal oxides (DMO) were used as catalytic supports and have proved to be very interesting materials due to their low cost and high possibilities of modification [29]. Zirconium phosphate heterostructure (PPH) presents high surface area values (450–600 $m^2\ g^{-1}$) due to the silica galleries within the phosphate layers that produce regular pores with diameters in the range of mesopores, as deduced by the type IV isotherms showed by them [30]. Moreover they possess moderate acidity (1.0–1.60 mmol $NH_3\ g^{-1}$) mainly due to the presence of P-O-H groups located on the layers of zirconium phosphate as well as to Si-O-H groups located on the surface of the silica galleries. This porous phosphate is a good catalyst support in HDO reactions using Pd-Nb as active phases [2]. This material also presented good results as catalyst support of ruthenium catalysts in the hydrogenation, hydrogenolysis, and hydrocracking of tetralin [31].

With these premises in mind, the aim of this paper was the preparation of bi-functional catalysts supported on a porous support—such is the case of zirconium phosphate heterostructure that also presents a high acidity—as well as the evaluation of their performance in the HDO reaction of dibenzofuran (DBF) as a model compound. This type of support provides an approach to achieve a high dispersion of the active phase, an interesting point in preparing highly active catalysts in this

type of reaction. Moreover, it was considered interesting to evaluate how the addition of Mo could affect the activity of noble metal based catalysts that present individually different catalytic behavior.

2. Results

2.1. Catalyst Characterization

The mesoporous phosphate heterostructure material (PPH) employed as support, is the result of the formation of silica galleries within the interlayer space of the CTMA expanded lamellar zirconium phosphate, MCM-50 type. After removing the surfactant by calcination, the structure was preserved and a porous material formed, which was reflected in the X-ray diffraction (XRD) pattern as a single peak at low angle corresponding to the d_{001} diffraction at ca. 40 Å (Figure A1). No diffraction lines were observed in the high angle region, indicating no co-precipitation of silica or zirconium phosphate during the process of synthesis of the support.

Figure 1 depicts the XRD patterns of the supported catalysts. In all cases a broad band at 2θ between 20° and 30°, which is characteristic of amorphous materials, is found. In the case of PdMo/PPH fresh and spent catalysts, no well-defined diffraction lines are observed in the high angle region, probably due to the high dispersion of the active phases, although it could be also explained by the low Pd and Mo loading, perhaps below the detection limit of the technique. As regards the PtMo/PPH catalyst, only two weak diffraction signals at 2θ = 39.7°, and 46.3°, assigned to metallic platinum (PDF 00-001-1190), can be observed, indicating the formation of metallic particles during the process of calcination; these signals remain unchanged after the catalytic HDO test. These results suggest a better dispersion of the metallic phase in the case of the Pd based catalyst. The diffraction peak at 2θ = 35.6° (PDF 01-074-2307) in both spent catalysts is due to the presence of silicon carbide (SiC) which was used as diluent in the preparation of the samples for the catalytic test.

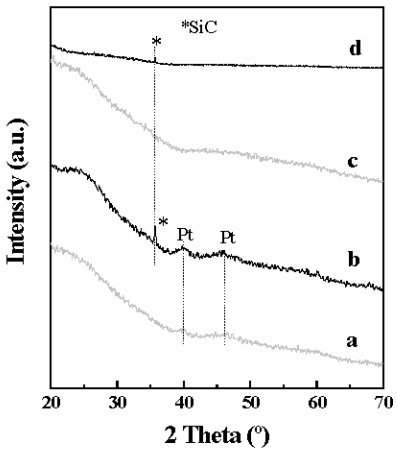

Figure 1. Diffractograms of: (**a**) PtMo/PPH fresh; (**b**) PtMo/PPH after reaction; (**c**) PdMo/PPH fresh; and (**d**) PdMo/PPH after reaction.

Transmission electron microscopy (TEM) study of the catalysts gives an idea of the degree of dispersion of the metallic phase on both catalysts, the corresponding micrographs are shown in Figure 2. For PdMo/PPH (Figure 2A,B), the images show the presence of highly dispersed small particles homogeneously distributed on the material support. Although some agglomerates are also observed, the majority of particles are in the range 1–2 nm (see Figure 3A). The same can be said about PtMo/PPH catalyst (Figure 2C,D), although the average particle size of the metallic fraction seems to be slightly higher (~2–3 nm) and the particle size distribution is wider than that observed for PdMo/PPH, as shown in Figure 3B. Furthermore, a greater number of agglomerates of large particles

were observed in this material. As previously observed from XRD, better active phase dispersion is achieved in the case of Pd catalyst.

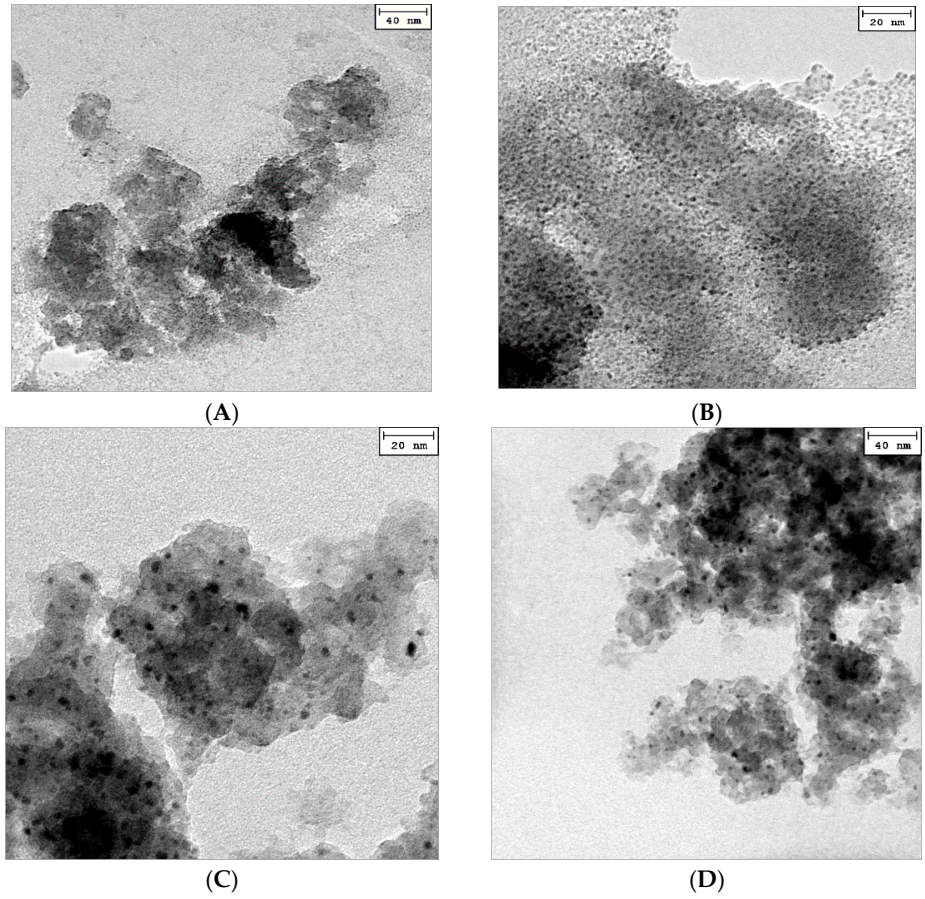

Figure 2. Micrographs corresponding to fresh catalysts: PdMo/PPH (**A**,**B**) and PtMo/PPH (**C**,**D**).

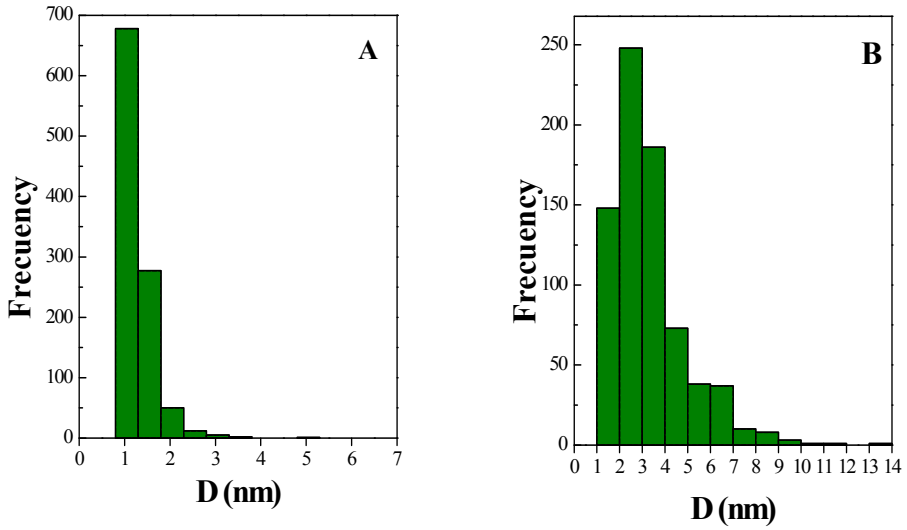

Figure 3. Particle size distribution corresponding to fresh PdMo/PPH (**A**) and PtMo/PPH (**B**) catalysts.

Moreover, additional micrographs in STEM mode were done in order to obtain mapping results of both samples as well as a quantification of Pt(Pd)-Mo in these samples (Figure 4).

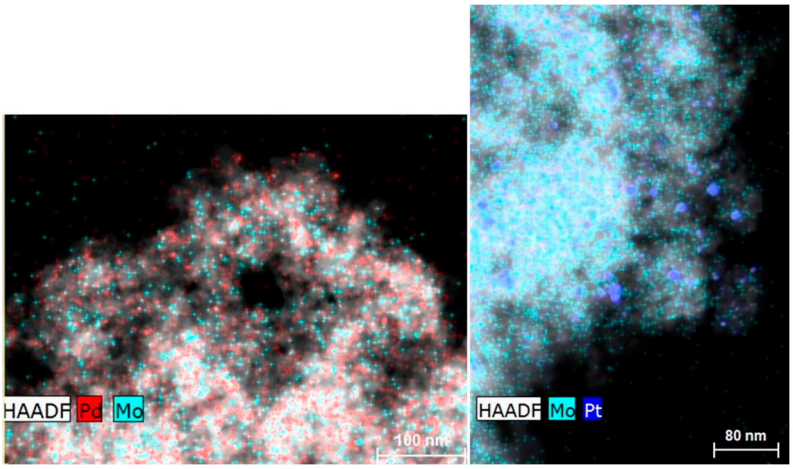

Figure 4. Mapping results corresponding to PdMo/PPH and PtMo/PPH.

Quantification results indicated that the compositions were similar to the nominal one, with Pd/Mo mean ratios of 1.05 and Pt/Mo ones of 0.98.

The textural properties of the support and catalysts were obtained from N_2 adsorption-desorption isotherms at −196 °C, and are depicted in Figure 5. In addition, Table 1 lists the corresponding textural properties derived from them.

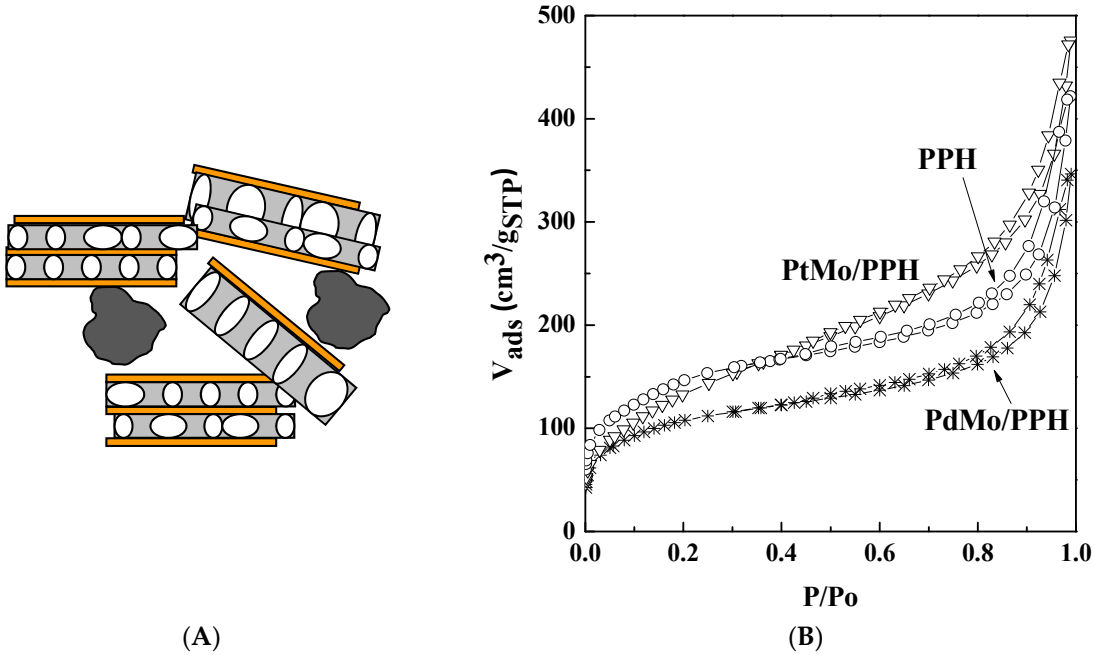

Figure 5. (**A**) Representation of additional pores by interaction of nanoparticles of bigger size. (**B**) N_2 adsorption-desorption isotherms of porous phosphate heterostructure (PPH) support and the corresponding supported fresh catalysts and schematic representation of the location of higher particles in the PPH structure.

All the isotherms are of type IV and exhibit a hysteresis loop, which is characteristic of mesoporous materials. The isotherm of PtMo/PPH catalyst is similar to that of the bare support [30]; however, the catalyst PdMo/PPH showed a decrease of the N_2 adsorbed over all the range of relative pressures studied. It is possible that a certain number of mesopores had been blocked by the entrance of Pd^0

particles, which, as it has been discussed, showed a very narrow distribution of sizes; furthermore, these particle sizes were always smaller than the average pore diameter of the bare material (Table 1).

Table 1. Lists the textural properties of the different samples prepared.

Sample	S_{BET} (m^2 g^{-1}) [a]	V_P (m^3 g^{-1}) [b]	d_p (nm) [c]
PPH	533	0.65	4.9
PdMo/PPH	388	0.53	5.5
PtMo/PPH	504	0.73	5.8

[a] S_{BET}: Brunauer, Emmett and Teller specific surface areas; [b] V_p: pore volume; [c] d_p: Mean pore diameter calculated from 4V/A equation. PPH = porous phosphate heterostructure.

In fact, by adding the active phase, the Pt-containing catalyst suffers only a slight loss in BET surface area value relative to the surface area presented by the pristine support, while this loss is much more remarkable in the case of the Pd-based catalyst. Instead, pore volume decreases in the latter, probably due to the main location of the small particles present in this material in smaller pores, mainly in the inner part of the silica galleries. The greater mean pore diameter of the catalysts compared to the bare support could be due to the formation of additional pores by interaction of nanoparticles of bigger size that cannot enter into the channels and are located outside between the packets' layers (see Picture 1 and Figure 5) [32]. This effect is more important for PtMo/PPH catalyst where the presence of larger particles is higher. In fact, a sharp increase is clearly observed in the adsorbed volume at high relative pressures.

The concentration of acid centers and strength were determined by NH_3-TPD. Table 2 shows the amount of desorbed NH_3 (μmol NH_3 g^{-1}) based catalysts supported of PdMo and PtMo and the fresh PPH support.

Table 2. Acidic properties of the fresh catalysts and support determined by NH_3-temperature-programmed desorption (TPD).

Sample	Acidity (μmol NH_3 g^{-1})				Acidity (μmol NH_3 m^{-2})
	Weak [a]	Average [b]	Strong [c]	Total	
PPH	494	285	38	817	1.53
PdMo/PPH	798	496	164	1459	3.76
PtMo/PPH	1070	553	135	1759	3.49

[a] NH_3 desorbed between 100 and 300 °C; [b] NH_3 desorbed between 300 and 500 °C; [c] NH_3 desorbed between 500 and 800 °C.

From these data, the moderate high acidity of these catalysts is due to the acidic nature of PPH and the incorporation of the active phases. Furthermore, the most important desorption occurs at low temperature, indicating that the acidity is mainly of a weak nature. Additionally, both catalysts show considerable amounts of NH_3 desorbed in the range 300–500 °C, indicating that they also possess average acidity. Finally, the amount of desorbed ammonia was normalized by the surface area of the sample. It can be seen that the amount of ammonia desorbed per m^2 of sample is higher for the catalysts, indicating that the addition of Pt, Pd, and Mo increased the acidity.

The surface chemical composition of the fresh catalysts and used catalysis was evaluated by XPS. Considering the Mo signal (Figure 6), in both cases two contributions due to the spin-orbit doublet of Mo 3*d* were observed, the binding energy of the Mo $3d_{5/2}$ component located at 232.3 eV for the Pt/Mo sample and 232.8 eV for the Pd/Mo sample. These values are slightly higher (between 0.3 and 0.9 eV), than that reported for MoO_3 [33], probably due to the greater interaction of the active phase with the carrier, being more acidic, as discussed below. The Mo 3*d* signal does not show significant changes after the catalytic process in the case of the Pt/Mo sample, and was not detected in the case of the Pd/Mo one.

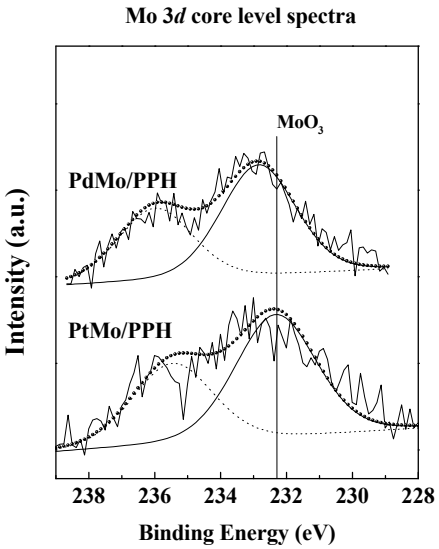

Figure 6. Core level spectra of Mo 3*d*.

The Pt 4*f* core level spectrum the PtMo/PPH catalyst shows two doublets, as can be clearly seen in Figure 7. The Pt $4f_{7/2}$ component located at 71.1 eV corresponds to metal Pt and that located at 72.5 eV is characteristic of the Pt^{2+} ion corresponding to PtO [34]. After catalysis, both of the two contributions due to Pt^0 and PtO are also observed, the contribution of the metallic phase being the most important one. The presence of PtO in the used catalyst is associated with the oxidation of Pt^0 by water, a byproduct of the reaction.

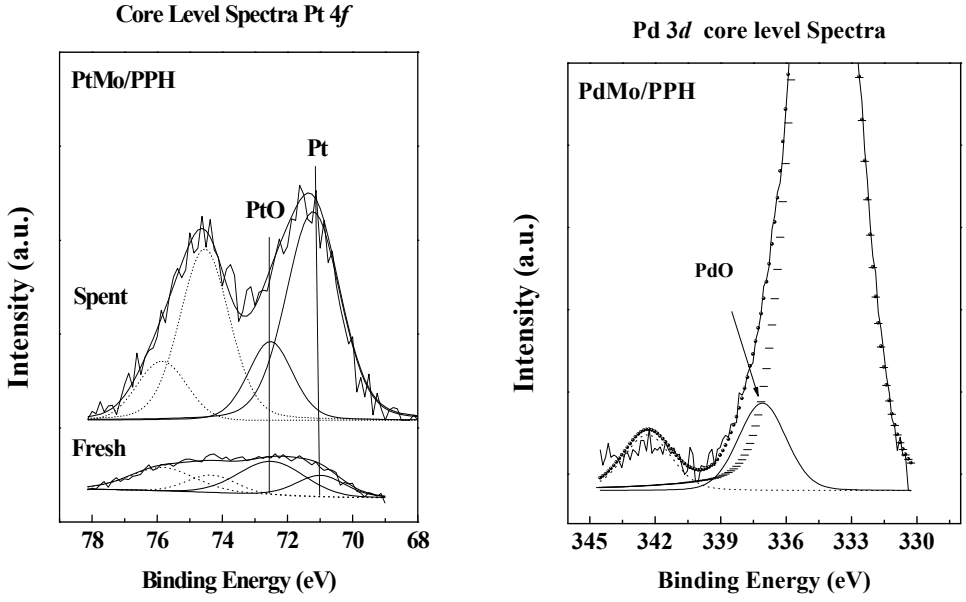

Figure 7. Core level spectra of Pt 4*f* and Pd 3*d*.

Figure 7 also shows the Pd 3*d* core level spectra. The spectrum for the catalyst PdMo/PPH fresh presents a contribution at 334.0 eV corresponding to the Zr 3*p* signal coming from the carrier. Furthermore, the presence of PdO is also observed with a Pd $3d_{5/2}$ contribution at 337.1 eV, as well as its corresponding doublet [35].

The surface atomic concentration of the elements is also included in Table 3. The catalyst containing Pt possesses larger Pt/Sup and Mo/Sup ratios than the Pd based one. On the other

hand, the atomic noble metal/Mo ratio, in both cases is lower than the nominal composition, 1, which points to a surface enrichment of Mo species, especially in the PdMo/PPH catalyst, having the lowest value.

Table 3. Binding energy values for Pd $3d_{5/2}$, Pt $4f_{7/2}$ and Mo $3d_{5/2}$.

Catalysts		Binding Energy (eV)			Atomic Surface Relations		
		Pd $3d_{5/2}$ Pt $4f_{7/2}$		Mo $3d_{5/2}$	Pd(Pt)/Mo	Pd(Pt)/Sup	Mo/Sup
		M°	MO_x	Mo(VI)			
PdMo/PPH	F	-	337.1	232.8	0.375	0.0020	0.0118
	U	-	-	-	-	-	-
PtMo/PPH	F	70.9	72.5	232.1	0.625	0.0031	0.0131
	U	71.2	72.5	232.5	0.692	0.0051	0.0074

F: fresh catalyst; U: used catalyst; M°: Pt or Pd; Mo: PtO or PdO; Sup: P + Zr + Si.

2.2. Catalytic Results

As it was stated previously, the synthesized catalysts were evaluated in the HDO reaction of dibenzofuran. The reaction was carried out at 275 °C and at two different pressures, 15 and 30 bar, to evaluate conversion as a function of reaction time. Figure 8 shows the comparison between both samples at both reaction pressures studied.

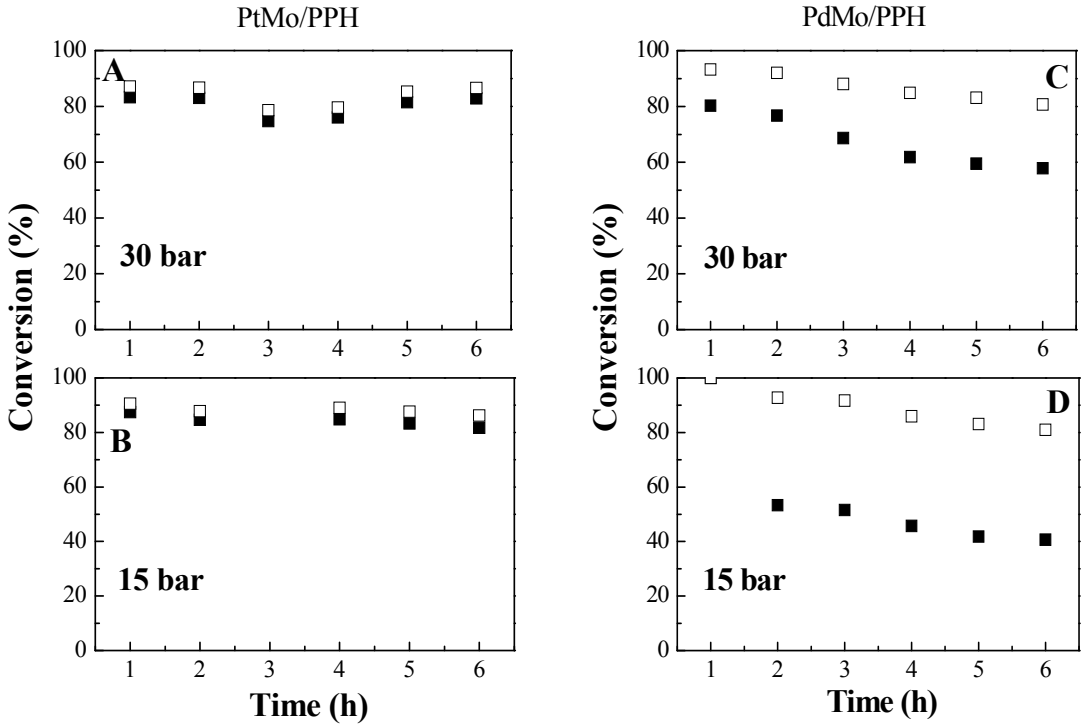

Figure 8. Evolution of the total (open symbols) and hydrodeoxygenation (HDO) (filled symbols) conversion with reaction time for: PtMo/PPH catalyst: (**A**) 30 bar and (**B**) 15 bar; PdMo/PPH catalyst: (**C**) 30 bar and (**D**) 15 bar. Reaction conditions: T = 275 °C, LHSV = 3.6 h^{-1}, GHSV = 7200 Ncc/g_{cat}h, H_2 contact time = 6 s, H_2/DBF = 69.1.

PtMo/PPH catalyst showed total and HDO conversions very similar, at around 80%. This catalyst shows a substantially constant conversion with the reaction time and the activity is similar at different

pressures. Very different is the behavior of the catalyst PdMo/PPH; that is, the total conversion is greater than the HDO conversion in both cases, showing a practically constant difference of 15% less compared to the total conversion in the reaction at 30 bar and practically 40% lower in the reaction at 15 bar. The conversion decreases with the reaction time and the conversion is higher at 30 than at 15 bar (see Figure 8). Moreover, HDO conversion is much more affected by the reaction pressure. These data indicate the important role of the active phase in these reactions. Thus, the presence of Pt improves the hydrogenolysis capability, being much more selective to O-free products. Instead, Pd shows greater hydrogenation ability and therefore is much more sensitive to reaction pressure conditions. It is of note that in the case of PtMo based catalyst, the H_2 pressure had no influence on the conversion, being practically equal to 80% at both pressures (Figure 8). Nevertheless, in the case of PdMo, the effect of hydrogen pressure is significant. After six hours of reaction (Figure 9) it is clearly observable.

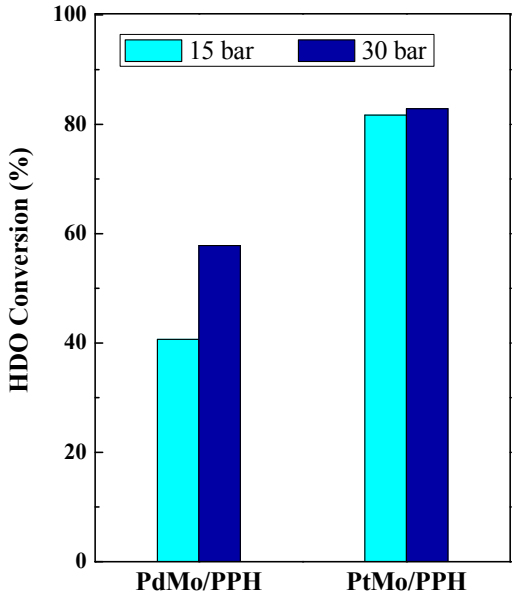

Figure 9. Comparison of HDO conversion at T.o.S. = 6h, for catalysts at 15 and 30 bar. Reaction conditions: T = 275 °C, LHSV = 3.6 h^{-1}, GHSV = 7200 Ncc/g_{cat}h, H_2 contact time = 6 s, H_2/DBF = 69.1.

In terms of catalyst stability, PtMo/PPH seems to achieve steady state conditions at both reaction pressures evaluated. PdMo/PPH suffers a decrease in both total and HDO conversion but the observed tendency is that after six hours on stream, it achieves a plateau. However, by studying the process of HDO of DBF, the main products obtained as non-oxygenated compounds were: bycyclohexane (BCH) and cyclohexane (CH) and in a lesser extent cyclohexylbenzene (CHB), cyclopentilcyclohexane (C-PE-CH), and cyclopentylmethylcyclohexane (C-PE-ME-CH). As intermediate oxygenates compounds 2,3,4,9 tetrahydrodibenzofuran (THDBF), 2,3,4,4a,9,9a hexahydrodibenzofuran (HHDBF), 2-cyclohexylphenol (2-CHP): 1-1-bi(cyclohexane)-3-en-2-ol isomers (BCH-3-en-2-ol), and bicyclohexane-2-ol (BCHol) were detected. Figures 10 and 11 compile the main reaction products obtained at 15 and 30 bar for PtMo/PPH and PdMo/PPH, respectively (Scheme 1).

For PtMo/PPH catalyst, the selectivity is similar at 15 and 30 bar. It can be observed that the major product obtained is BCH with selectivity almost constant between 60% and 70%. CH is the second major non-oxygenated product obtained with a proportion of about 20% during the whole time of the reaction. Other non-oxygenated products such as CBH, C-PE-ME-OH, and C-PE-CH, were obtained in a proportion of less than 5% for both reaction pressures. In both reactions, oxygenated products (THDBF, HHDBF, 2-CHP, BCH-3-en-2-ol) were detected in a proportion of less than 3%.

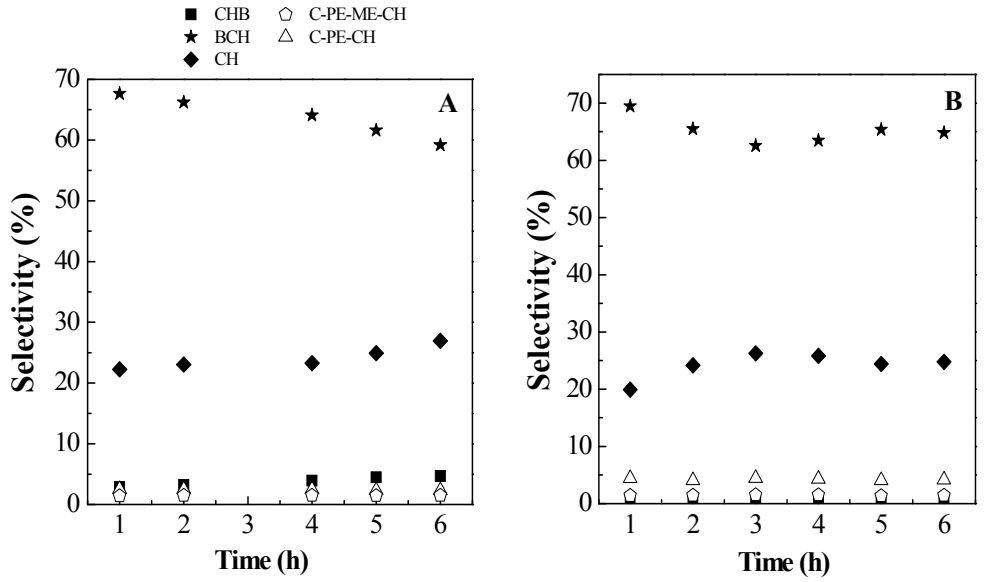

Figure 10. Selectivity values to the reaction products for PtMo/PPH catalyst at: (**A**) 15 bar and (**B**) 30 bar. Reaction conditions: T = 275 °C, LHSV = 3.6 h^{-1}, GHSV = 7200 Ncc/g_{cat}h, H_2 contact time = 6 s, H_2/DBF = 69.1.

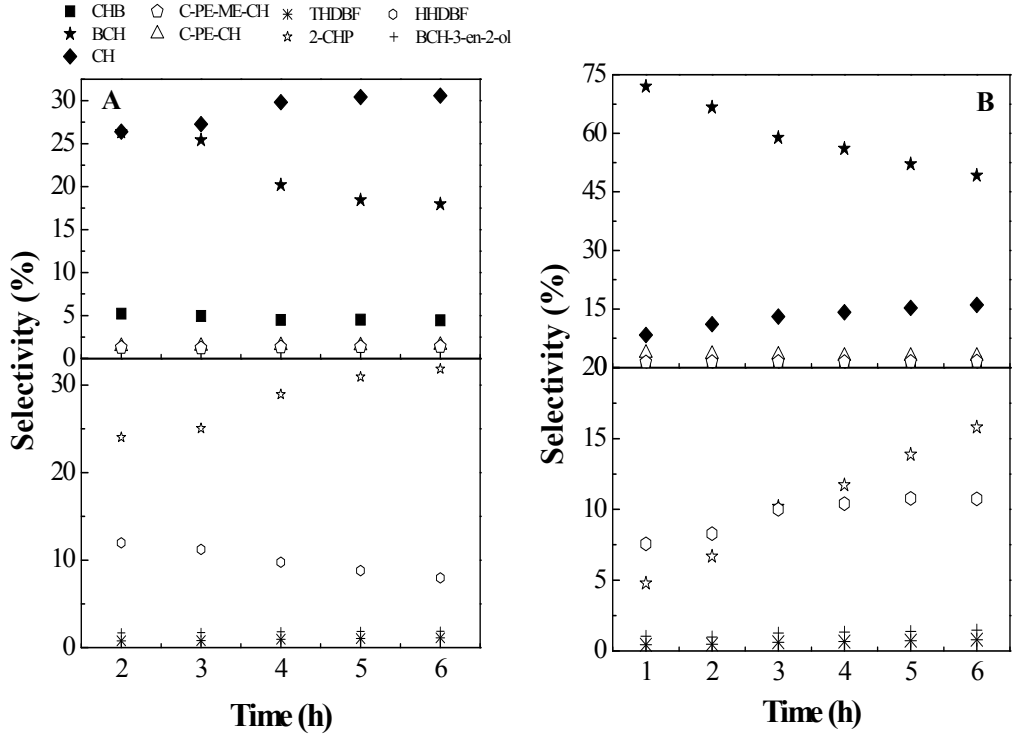

Figure 11. Selectivity values for the reaction products for PdMo/PPH catalyst at: (**A**) 15 bar and (**B**) 30 bar. Reaction conditions: T = 275 °C, LHSV = 3.6 h^{-1}, GHSV = 7200 Ncc/g_{cat}h, H_2 contact time = 6 s, H_2/DBF = 69.1.

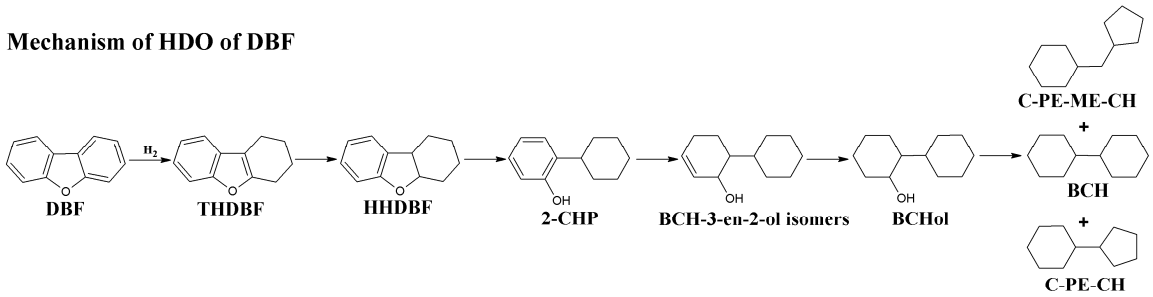

Scheme 1. Possible mechanisms of HDO reaction for dibenzofuran [5,34].

In the case of PdMo/PPH catalyst (Figure 11), it can be seen that the main deoxygenated products at 15 bar were CH and BCH; however, as the reaction proceeds, the major product is CH, while the BCH selectivity decreases. Conversely, at 30 bar, the main product is BCH, but BCH selectivity decreases with reaction time similar to that observed at 15 bar. These data indicate that the reaction pressure has an important role in the reaction products for the Pd catalyst. So, at 15 bar, the BCH molecule may break and cause CH, while this break appears inhibited at 30 bar. Furthermore, BCH selectivity decreases slightly while increasing the selectivity to 2-CHP. This points to the blockage of the sites where the CO bond rupture takes place.

Regarding the selectivity towards oxygenated intermediates, at 15 bar, the main compound is 2-CHP. At 30 bar, where the selectivity to these products is lower, the major product is initially HHDBF and after 6 h of reaction, the selectivity to 2-CHP is greater.

Selectivity data after six hours of reaction (Figure 12) indicate that the catalyst with better selectivity is that based on Pt. Furthermore, it is noted that this catalyst is the most selective toward deoxygenated compounds as BCH and CHB, and CH to a lesser extent. As oxygenate compound, a minimum amount of 2-CHP is formed. The amount of other species formed is not significant. It is also of note that the selectivity towards deoxygenated compounds is slightly greater at 30 bar than that at 15 bar, which coincides with the yields obtained for this catalyst. The catalyst based on Pd showed a CH selectivity close to 2-CHP at both pressures. Only when the pressure is higher, the selectivity towards non oxygenated products is higher than 60%. Another oxygenated compound, HHDBF, is also formed in relative high quantity, at both pressures. The rest of the non-oxygenated products were obtained in a proportion less than 2%.

Therefore, catalysts based on Pt gave better results than Pd catalysts. The pressure had a significant effect on the selectivity distribution of deoxygenated product, mainly BCH. CH was obtained at both pressures with a selectivity of around 20%–30%, and depending on the reaction pressure. Both catalysts were able to hydrogenate and deoxygenate the DBF to BCH, and also were able to dissociate the molecule to form CH. Moreover, the Pt based sample did not show deactivation during the catalytic reaction of HDO, while PdMo suffered a decrease in its activity. Furthermore, it was found that, while catalysts based on PtMo had no significant change of activity with variations in pressure, those based on PdMo improved operation by increasing the reaction pressure.

If the results are compared (see Table 4) with those obtained with a non-acidic and commercial support such as silica (fumed silica from Aldrich, St. Louis, MO, USA), it can be seen that the Pt based catalyst showed a lower conversion when supported on SiO_2 although PtMo/SiO_2 was more selective to BCH and CH. Moreover, the total percentage of deoxygenated products was higher with the PtMo/PPH sample. In the case of PdMo/SiO_2, it can be seen that the HDO conversion and selectivity towards deoxygenated compounds is higher than for PdMo/PPH. However, the latter is much more selective to CH.

These results highlight the importance of both, noble metal and support in this reaction. PPH material can be considered a good candidate as catalyst support, since high conversion and selectivity

values are attained in both cases and the results are comparable or even better than those achieved with a commercial support.

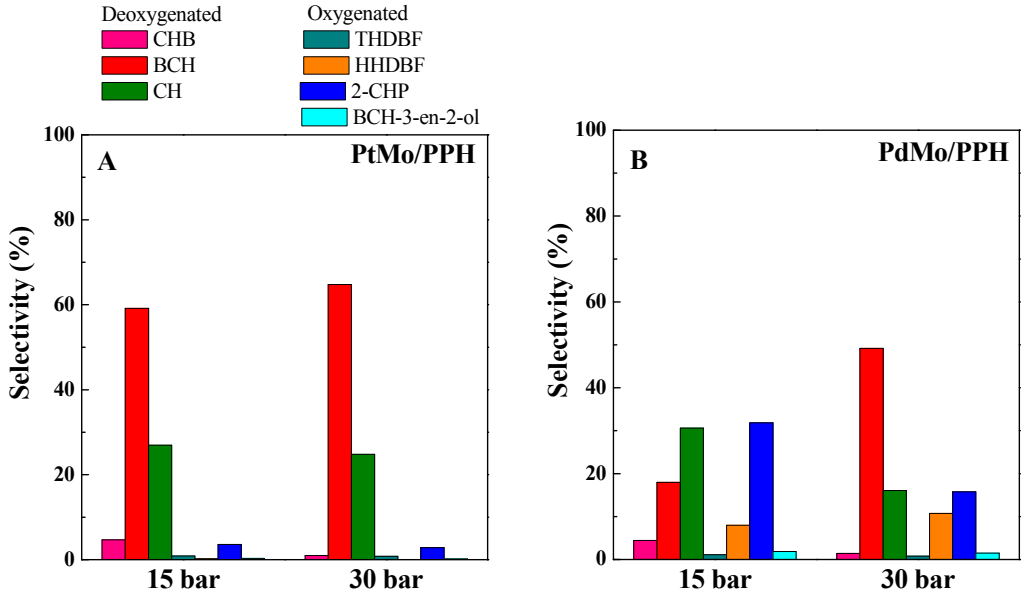

Figure 12. Selectivity values for the reaction products obtained with each catalyst and after six hours of reaction for PtMo/PPH catalyst (**A**) and PdMo/PPH catalyst (**B**). Reaction conditions: T = 275 °C, LHSV = 3.6 h^{-1}, GHSV = 7200 Ncc/g_{cat}h, H_2 contact time = 6 s, H_2/DBF = 69.1961.

Table 4. Conversion and Selectivity for PtMo and PdMo supported catalysts supported on PPH and SiO_2.

	Conversion (%)		Selectivity (%)		
Sample	**HDO**	**Total**	**BCH**	**CH**	**CHB**
PtMo/PPH	81.66	86.21	59.2	26.9	4.7
PtMo/SiO_2	74.98	84.21	69.0	0.5	12.3
PdMo/PPH	40.6	80.9	18.0	30.6	4.4
PdMo/SiO_2	56.5	90.9	46.1	0.5	11.4

Reaction conditions: T.o.S. = 6 h, P: 15 bar, T: 275 °C, LHSV = 3.6 h^{-1}, GHSV = 7200 Ncc/g_{cat}h, H_2 contact time = 6 s, H_2/DBF = 69.1.

3. Materials and Methods

3.1. Preparation of Catalysts

Pt(Pd)/Mo supported catalysts on PPH material were prepared by following the incipient wetness impregnation method. The PPH support was synthesized employing hexadecylamine/P and tetra-ethylorthosilicate (TEOS)/P molar ratios of 0.2 and 3.0, respectively, according to the procedure described by Jiménez-Jimenez et al. [30]. Briefly, the synthesis was carried out by using cetyltrimethylammonium (CTMA)-expanded zirconium phosphate as precursor, which was prepared with a solution of CTMABr in *n*-propanol, H_3PO_4 and zirconium(IV) *n*-propoxide. The resultant solution was stirred for four days at room temperature. The obtained solid (CTMA–ZrP), obtained by filtration, was suspended in water and stirred two days at room temperature. After which, it was added as co-surfactant hexadecylamine in *n*-propanol. After 1 day under stirring, a solution of TEOS in n-propanol was added as reactant to generate the silica galleries. This suspension was stirred at room temperature for 3 days. The solid obtained was then centrifuged, washed with ethanol, and

dried at 60 °C in air. This as-prepared material was calcined at 550 °C for 6 h to remove the surfactant used as template and generate the porosity to obtain the PPH material.

The solid was then impregnated with aqueous solutions containing the proper concentrations of Pt and Mo or Pd and Mo precursor salts ($(NH_4)_2PtCl_4$ 99.9% and $PdCl_2$ 99.9% from Aldrich; $(NH_4)_6Mo_7O_{24}{\cdot}4H_2O$, 99%, from Alfa Aesar, Ward Hill, MA, USA); in the case of $PdCl_2$ containing solution, HCl aqueous concentrated acid was also added, in order to keep palladium(II) species in solution. The materials were dried at 60 °C for 12 h and finally calcined at 450 °C for 2 h. The obtained catalysts were denoted as PtMo and PdMo. Both samples contained a total metallic loading (Pt or Pd and Mo) of 2 wt % and Pt(Pd)/Mo atomic ratio equal to 1.

3.2. Characterization of Catalysts

The catalysts were characterized without previous reduction pretreatment, i.e., the as prepared samples. The prepared catalysts were characterized by X-ray diffraction in an X'Pert Pro MPD automated diffractometer (PAN analytical). Powder patterns were recorded between 20° and 70° in 2θ, with a step size of 0.0167° (2θ) and an equivalent counting time of ∼60 s/step, in Bragg-Brentano reflection configuration by using a Ge (111) primary monochromator, using monochromatic Cu Kα radiation (λ = 1.5406 Å) and an X'Celerator detector. Brunauer, Emmett and Teller (BET) specific surface areas were obtained from nitrogen adsorption-desorption measurements at −196 °C on a Micrometric ASAP 2020 apparatus, with all samples previously degassed at 200 °C for 10 h. The acidity of pure support and prepared catalysts was determined by temperature-programmed desorption (TPD) of ammonia measurements from 100 °C to 800 °C, employing He as gas carrier and a TCD detector. The reducibility of the samples was studied by temperature-programmed reduction in flowing H_2 (RTP-H_2); each sample was cleaned in a flow of He (35 mL/min) at 100 °C for half an hour; after cooling the furnace to 45 °C, samples were then heated in a H_2 flow (45 mL/min) to 700 °C using a heating ramp of 10 °C/min; The measurement was recorded on a Shimadzu GC-14b chromatograph. The fresh catalysts were studied by High-Resolution Transmission Electron Microscopy (HRTEM) was carried out using a Philips CCCM 200 Supertwin-DX4 microscope. Scanning transmission electron microscopy (STEM) analysis and mapping data were recorded in a TALOS F200x instrument with a high-angle annular dark field (HAADF) detector, at 200 kV and 200 nA. The particle size estimation was obtained by using ImageJ software sampling at least 700 particles for each material. The microanalysis was carried out with Energy dispersive X-ray Spectroscopy (EDAX) Super-X system provided with four X-ray detectors and an X-FEG beam. A Physical Electronics PHI 5701 spectrometer was used to obtain the catalysts X-ray photoelectron spectra (XPS); a non monochromatic Mg-Kα radiation (300 W, 15 kV, 1253.6 eV) and a multi-channel detector were employed.

3.3. Catalytic Activity

The catalytic activity of the prepared catalysts in the HDO reaction was evaluated employing a high-pressure fixed-bed catalytic reactor and dibenzofuran (DBF) as model molecule. To this end, 0.25 g of catalyst (particle size 0.85–1.00 mm), diluted with silicon carbide to achieve a total volume of 3 cm^3, was used. The reactions were carried out at 275 °C under 3.0 and 1.5 MPa of H_2; the H_2 flow being 30 mL min^{-1} and the organic feed flow 0.18 mL min^{-1} (supplied with a Gilson 307SC piston pump). The LHSV (Reactant Liquid Flow Rate/Reactor Volume) was 3.6 h^{-1}, and the GHSV (Reactant Gas Flow Rate/Reactor Volume) was 7200 Ncc/g_{cat}h. Carbon balances were in the range of 1.00 +/− 0.05.

The activity is described in terms of the HDO conversion according to Equation (1):

$$X_{HDO} = \frac{n_{0h} - \sum n_{oxi}}{n_{0h}} \cdot 100 \quad (1)$$

where n_{0h} is the initial amount of DBF and n_{oxi} is the amount of oxygenated compounds (all of them expressed in moles).

For better understanding of the activity, total conversion is defined according to Equation (2):

$$X_{Total} = \frac{n_{oh} - n_{fh}}{n_{oh}} \cdot 100 \quad (2)$$

where n_{fh} is the final amount of DBF.

4. Conclusions

Pd(Pt)/Mo catalysts supported on porous phosphate heterostructure and prepared by incipient wetness impregnation were investigated in the hydrodeoxygenation of the dibenzofuran reaction. Characterization results showed that a high dispersion of the active phase was achieved in both cases, and mainly in the case of Pd, with a particle size distribution between 1 and 2 nm. The lower particle size of the Pd catalyst caused a decrease of the pore volume of the material due to the preferential location in the pores of smaller size. Moreover, mapping results also indicate that Mo and Noble metal are both homogeneously dispersed on the catalyst surface. On the other hand, the larger particles of Pt did not enter into the support channels and create new holes that lead to a higher adsorbed volume at high pressures and a larger BET surface area. Catalytic results evidenced, that the active phase is that governing the catalytic behavior of these systems. Thus, the catalyst based on Pt presented a better yield for non-oxygenated compounds, showing conversions near 80%. Instead, the Pd based catalyst showed worse results than the Pt one in terms of conversion, but presented better hydrogenation properties, being much more affected by changes in hydrogen pressures than the Pt one. Thus, the Pt catalyst was able to hydrogenate and deoxygenate the molecule of DBF to obtain BCH molecule, regardless of the reaction pressure employed. Moreover, both samples presented high selectivity values to CH, indicating that these catalysts were able to dissociate the BCH molecule. This effect was not observed with a non-acidic and commercial support.

Acknowledgments: Thanks to projects CTQ2015-68951-C3-3R (Ministerio de Economía y Competitividad, Spain and FEDER Funds) and P12-RNM-1565 (Junta de Andalucía, Spain). A.I.M. thanks the Ministry of Economy and Competitiveness for a Ramón y Cajal contract (RyC2015-17870).

Author Contributions: Daniel Ballesteros-Plata, Antonia Infantes-Molina and Enrique Rodríguez-Castellón conceived and designed the experiments; Daniel Ballesteros-Plata and Elena Rodríguez-Aguado performed the experiments; Antonia Infantes-Molina, Pilar Braos-García, José Jiménez-Jiménez analysed the data; Daniel Ballesteros-Plata and Elena Rodríguez-Aguado contributed reagents/materials/analysis tools; and Daniel Ballesteros-Plata, Antonia Infantes-Molina, Pilar Braos García and Enrique Rodríguez-Castellón wrote the paper.

Conflicts of Interest: The authors declare no conflict of interest.

Appendix A

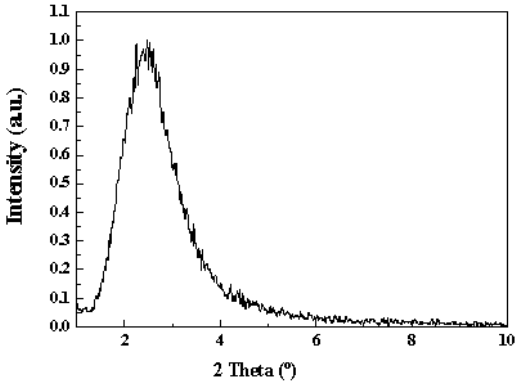

Figure A1. XRD patern of PPH support.

References

1. Demirbaş, A. Biomass resource facilities and biomass conversion processing for fuels and chemicals. *Energy Convers. Manag.* **2001**, *42*, 1357–1378. [CrossRef]
2. Infantes-Molina, A.; Moretti, E.; Segovia, E.; Lenarda, A.; Rodríguez-Castellón, E. Pd-nb binfunctional catalysts supported on silica and zirconium phosphate heterostructures for o-removal of dibenzofurane. *Catal. Today* **2016**, *277*, 143–151. [CrossRef]
3. Bridgwater, A.V.; Meier, D.; Radlein, D. An overview of fast pyrolysis of biomass. *Org. Geochem.* **1999**, *30*, 1479–1493. [CrossRef]
4. Boullosa-Eiras, S.; Lødeng, R.; Bergem, H.; Stöcker, M.; Hannevold, L.; Blekkan, E.A. Catalytic hydrodeoxygenation (hdo) of phenol over supported molybdenum carbide, nitride, phosphide and oxide catalysts. *Catal. Today* **2014**, *223*, 44–53. [CrossRef]
5. Furimsky, E. Catalytic hydrodeoxygenation. *Appl. Catal. A Gen.* **2000**, *199*, 147–190. [CrossRef]
6. Echeandia, S.; Pawelec, B.; Barrio, V.L.; Arias, P.L.; Cambra, J.F.; Loricera, C.V.; Fierro, J.L.G. Enhancement of phenol hydrodeoxygenation over pd catalysts supported on mixed hy zeolite and Al_2O_3. An approach to o-removal from bio-oils. *Fuel* **2014**, *117*, 1061–1073. [CrossRef]
7. Han, Y.; McIlroy, D.N.; McDonald, A.G. Hydrodeoxygenation of pyrolysis oil for hydrocarbon production using nanospring based catalysts. *J. Anal. Appl. Pyrolysis* **2016**, *117*, 94–105. [CrossRef]
8. Mortensen, P.M.; Grunwaldt, J.D.; Jensen, P.A.; Knudsen, K.G.; Jensen, A.D. A review of catalytic upgrading of bio-oil to engine fuels. *Appl. Catal. A Gen.* **2011**, *407*, 1–19. [CrossRef]
9. Lee, H.W.; Jun, B.R.; Kim, H.; Kim, D.H.; Jeon, J.-K.; Park, S.H.; Ko, C.H.; Kim, T.-W.; Park, Y.-K. Catalytic hydrodeoxygenation of 2-methoxy phenol and dibenzofuran over pt/mesoporous zeolites. *Energy* **2015**, *81*, 33–40. [CrossRef]
10. Bu, Q.; Lei, H.; Zacher, A.H.; Wang, L.; Ren, S.; Liang, J.; Wei, Y.; Liu, Y.; Tang, J.; Zhang, Q.; et al. A review of catalytic hydrodeoxygenation of lignin-derived phenols from biomass pyrolysis. *Bioresour. Technol.* **2012**, *124*, 470–477. [CrossRef] [PubMed]
11. Patel, M.; Kumar, A. Production of renewable diesel through the hydroprocessing of lignocellulosic biomass-derived bio-oil: A review. *Renew. Sustain. Energy Rev.* **2016**, *58*, 1293–1307. [CrossRef]
12. De la Puente, G.; Gil, A.; Pis, J.J.; Grange, P. Effects of support surface chemistry in hydrodeoxygenation reactions over como/activated carbon sulfided catalysts. *Langmuir* **1999**, *15*, 5800–5806. [CrossRef]
13. Dong, P.; Lu, G.-P.; Cai, C. Effective hydrodeoxygenation of dibenzofuran by a bimetallic catalyst in water. *New J. Chem.* **2016**, *40*, 1605–1609. [CrossRef]
14. Yohe, S.L.; Choudhari, H.J.; Mehta, D.D.; Dietrich, P.J.; Detwiler, M.D.; Akatay, C.M.; Stach, E.A.; Miller, J.T.; Delgass, W.N.; Agrawal, R.; et al. High-pressure vapor-phase hydrodeoxygenation of lignin-derived oxygenates to hydrocarbons by a ptmo bimetallic catalyst: Product selectivity, reaction pathway, and structural characterization. *J. Catal.* **2016**, *344*, 535–552. [CrossRef]
15. Ardiyanti, A.R.; Gutierrez, A.; Honkela, M.L.; Krause, A.O.I.; Heeres, H.J. Hydrotreatment of wood-based pyrolysis oil using zirconia-supported mono- and bimetallic (pt, pd, rh) catalysts. *Appl. Catal. A Gen.* **2011**, *407*, 56–66. [CrossRef]
16. Gutierrez, A.; Kaila, R.K.; Honkela, M.L.; Slioor, R.; Krause, A.O.I. Hydrodeoxygenation of guaiacol on noble metal catalysts. *Catal. Today* **2009**, *147*, 239–246. [CrossRef]
17. Wang, Y.; Fang, Y.; He, T.; Hu, H.; Wu, J. Hydrodeoxygenation of dibenzofuran over noble metal supported on mesoporous zeolite. *Catal. Commun.* **2011**, *12*, 1201–1205. [CrossRef]
18. Wang, L.; Li, C.; Jin, S.; Li, W.; Liang, C. Hydrodeoxygenation of dibenzofuran over sba-15 supported pt, pd, and ru catalysts. *Catal. Lett.* **2014**, *144*, 809–816. [CrossRef]
19. Halasz, I.; Brenner, A.; Shelef, M. Catalytic reduction of nitric oxide on pdo—MoO_3/γ-Al_2O_3. *Appl. Catal. B Environ.* **1993**, *2*, 131–146. [CrossRef]
20. Wang, L.; Zhang, M.; Zhang, M.; Sha, G.; Liang, C. Hydrodeoxygenation of dibenzofuran over mesoporous silica cok-12 supported palladium catalysts. *Energy Fuels* **2013**, *27*, 2209–2217. [CrossRef]
21. Mortensen, P.M.; Grunwaldt, J.-D.; Jensen, P.A.; Jensen, A.D. Screening of catalysts for hydrodeoxygenation of phenol as a model compound for bio-oil. *ACS Catal.* **2013**, *3*, 1774–1785. [CrossRef]

22. Shetty, M.; Murugappan, K.; Prasomsri, T.; Green, W.H.; Román-Leshkov, Y. Reactivity and stability investigation of supported molybdenum oxide catalysts for the hydrodeoxygenation (hdo) of m-cresol. *J. Catal.* **2015**, *331*, 86–97. [CrossRef]
23. Nolte, M.W.; Zhang, J.; Shanks, B.H. Ex situ hydrodeoxygenation in biomass pyrolysis using molybdenum oxide and low pressure hydrogen. *Green Chem.* **2016**, *18*, 134–138. [CrossRef]
24. Prasomsri, T.; Nimmanwudipong, T.; Román-Leshkov, Y. Effective hydrodeoxygenation of biomass-derived oxygenates into unsaturated hydrocarbons by MoO_3 using low H_2 pressures. *Energy Environ. Sci.* **2013**, *6*, 1732. [CrossRef]
25. Prasomsri, T.; Shetty, M.; Murugappan, K.; Román-Leshkov, Y. Insights into the catalytic activity and surface modification of MoO_3 during the hydrodeoxygenation of lignin-derived model compounds into aromatic hydrocarbons under low hydrogen pressures. *Energy Environ. Sci.* **2014**, *7*, 2660. [CrossRef]
26. Robinson, A.; Ferguson, G.A.; Gallagher, J.R.; Cheah, S.; Beckham, G.T.; Schaidle, J.A.; Hensley, J.E.; Medlin, J.W. Enhanced hydrodeoxygenation ofm-cresol over bimetallic pt–mo catalysts through an oxophilic metal-induced tautomerization pathway. *ACS Catal.* **2016**, *6*, 4356–4368. [CrossRef]
27. Ardiyanti, A.R.; Khromova, S.A.; Venderbosch, R.H.; Yakovlev, V.A.; Melián-Cabrera, I.V.; Heeres, H.J. Catalytic hydrotreatment of fast pyrolysis oil using bimetallic ni–cu catalysts on various supports. *Appl. Catal. A Gen.* **2012**, *449*, 121–130. [CrossRef]
28. Bui, V.N.; Laurenti, D.; Delichère, P.; Geantet, C. Hydrodeoxygenation of guaiacol. *Appl. Catal. B Environ.* **2011**, *101*, 246–255. [CrossRef]
29. Yan, K.; Liu, Y.; Lu, Y.; Chai, J.; Sun, L. Catalytic application of layered double hydroxide-derived catalysts for the conversion of biomass-derived molecules. *Catal. Sci. Technol.* **2017**, *7*, 1622–1645. [CrossRef]
30. Jiménez-Jiménez, J.; Rubio-Alonso, M.; Quesada, D.E.; Rodríguez-Castellón, E.; Jiménez-López, A. Synthesis and characterisation of acid mesoporous phosphate heterostructure (PPH) materials. *J. Mater. Chem.* **2005**, *15*, 3466. [CrossRef]
31. Eliche-Quesada, D.; Macías-Ortiz, M.I.; Jiménez-Jiménez, J.; Rodríguez-Castellón, E.; Jiménez-López, A. Catalysts based on ru/mesoporous phosphate heterostructures (PPH) for hydrotreating of aromatic hydrocarbons. *J. Mol. Catal. A Chem.* **2006**, *255*, 41–48. [CrossRef]
32. León, M.; Jiménez-Jiménez, J.; Jiménez-López, A.; Rodríguez-Castellón, E.; Soriano, D.; López Nieto, J.M. Vanadium oxide-porous phosphate heterostructure catalysts for the selective oxidation of h2s to sulphur. *Solid State Sci.* **2010**, *12*, 996–1001. [CrossRef]
33. Infantes-Molina, A.; Mérida-Robles, J.; Rodríguez-Castellón, E.; Fierro, J.L.G.; Jiménez-López, A. Effect of molybdenum and tungsten on co/msu as hydrogenation catalysts. *J. Catal.* **2006**, *240*, 258–267. [CrossRef]
34. Kozlova, E.A.; Lyubina, T.P.; Nasalevich, M.A.; Vorontsov, A.V.; Miller, A.V.; Kaichev, V.V.; Parmon, V.N. Influence of the method of platinum deposition on activity and stability of pt/TiO_2 photocatalysts in the photocatalytic oxidation of dimethyl methylphosphonate. *Catal. Commun.* **2011**, *12*, 597–601. [CrossRef]
35. Beketov, G.; Heinrichs, B.; Pirard, J.P.; Chenakin, S.; Kruse, N. Xps structural characterization of pd/SiO_2 catalysts prepared by cogelation. *Appl. Surf. Sci.* **2013**, *287*, 293–298. [CrossRef]